

pubs.acs.org/Macromolecules Article

Miscible Polyether/Poly(ether-acetal) Electrolyte Blends

Kevin W. Gao, Whitney S. Loo, Rachel L. Snyder, Brooks A. Abel, Youngwoo Choo, Andrew Lee, Susana C. M. Teixeira, Bruce A. Garetz, Geoffrey W. Coates,* and Nitash P. Balsara*



Cite This: Macromolecules 2020, 53, 5728-5739



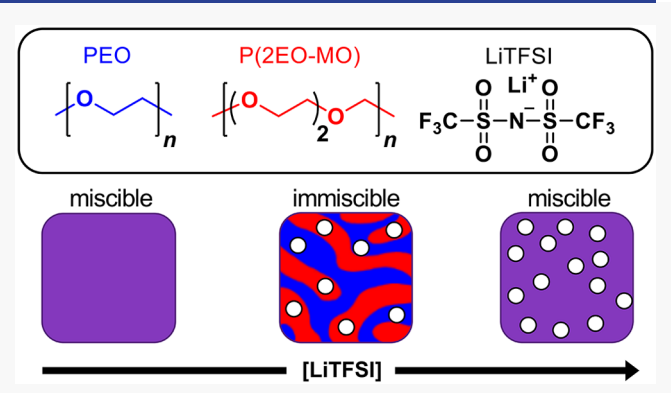
ACCESS

III Metrics & More

Article Recommendations

Supporting Information

ABSTRACT: This study shows that it is possible to obtain homogeneous mixtures of two chemically distinct polymers with a lithium salt for electrolytic applications. This approach is motivated by the success of using mixtures of organic solvents in modern lithium-ion batteries. The properties of mixtures of a polyether, poly(ethylene oxide) (PEO), a poly(ether—acetal), poly(1,3,6-trioxocane) (P(2EO-MO)), and lithium bis(trifluoromethanesulfonyl)imide (LiTFSI) salt were studied by small-angle neutron scattering (SANS) and electrochemical characterization in symmetric cells. The SANS data are used to determine the miscibility window and quantify the effect of added salt on the thermodynamic interactions between the polymers. In the absence of salt, PEO/P(2EO-MO) blends are homogeneous and



characterized by attractive interactions, i.e., a negative Flory–Huggins interaction parameter, χ . The addition of small amounts of salt results in a positive effective Flory–Huggins interaction parameter, $\chi_{\rm eff}$, and macrophase separation. Surprisingly, miscible blends and negative $\chi_{\rm eff}$ parameters are obtained when the salt concentration is increased beyond a critical value. The electrochemical properties of PEO/P(2EO-MO)/LiTFSI blends at a given salt concentration were close to those obtained in PEO/LiTFSI electrolytes at the same salt concentration. This suggests that in the presence of PEO the electrochemical properties exhibited by P(2EO-MO) chains are similar to those of PEO chains. This work opens the door to a new direction for creating new and improved polymer electrolytes either by combining existing polymers and salt or by synthesizing new polymers with the specific aim of including them in miscible polymer blend electrolytes.

■ INTRODUCTION

There is considerable interest in replacing flammable organic solvents with nonvolatile polymers in rechargeable lithium batteries. It has long been recognized that high dielectric constant and low viscosity are necessary for rapid ion transport in liquid electrolytes. In the case of lithium-ion batteries designed to operate at room temperature, this is achieved by blending materials. Ethylene carbonate has a dielectric constant of 89.8 but is a solid at room temperature (mp = $36.4~^{\circ}\text{C}$) while dimethyl carbonate is a low-viscosity liquid (mp = $4.6~^{\circ}\text{C}$) but has a dielectric constant of $3.1.^{1}$ Neither is a suitable solvent for electrolytic applications. However, a blend of ethylene carbonate and dimethyl carbonate is an excellent solvent for these applications and is a major component of lithium-ion battery electrolytes.

Translating the notion of liquid electrolyte mixtures to polymer electrolyte blends is nontrivial. While most low molar mass liquids are miscible with each other (e.g., polar molecules like ethanol are miscible in nonpolar liquids such as hexanes), finding pairs of miscible polymers is extremely rare. ^{2,3} Polymers with seemingly minor differences in monomer structure are entirely immiscible. For example, the solubility of polyethylene in polypropylene (both polymers have

empirical formulas CH_2) is negligible. The reason for this is well established: mixing is usually promoted by entropic considerations. The entropic gain of mixing polymers with long chains, however, is orders of magnitude smaller due to the connectivity of the monomers.

The purpose of this paper is to demonstrate that it is possible to create homogeneous mixtures of polymers with different polarities to create a new type of material for use in lithium batteries: miscible polymer blend electrolytes.

Our system of interest is a blend of a polyether, poly(ethylene oxide) (PEO), a poly(ether—acetal), poly-(1,3,6-trioxocane) (P(2EO-MO)), and lithium bis(trifluoromethanesulfonyl)imide (LiTFSI) salt (see Figure 1). PEO has been thoroughly studied as a potential electrolyte for lithium batteries due to its nonvolatility, electrochemical stability, and compatibility with lithium salts. 6-8 The ability of PEO to

Received: March 30, 2020 Revised: June 5, 2020 Published: July 10, 2020





P(2EO-MO)
$$\left\{ \begin{array}{c} O \\ 2 \end{array} \right\}_r$$

$$\begin{array}{cccc} & & \text{Li}^{\dagger} \\ \text{O} & \text{O} \\ \text{C} & \text{S} \\ \text{C} & \text{S} \\ \text{O} & \text{O} \\ \end{array}$$

Figure 1. Chemical structure of poly(ethylene oxide) (PEO), poly(1,3,6-trioxocane) (P(2EO-MO)), and lithium bis(trifluoromethanesulfonyl)imide (LiTFSI).

dissolve lithium salts is due to the presence of oxygen-containing ether linkages. The properties of P(2EO-MO)/LiTFSI electrolytes were reported in ref 9. We expect P(2EO-MO) to be more polar than PEO due to the increased concentration of ether and acetal oxygens. Ternary blends with polymer components of different polarities have been discussed as a means for improving ion transport in a recent theoretical paper by using a coarse-grained bead—spring model. ¹⁰

In this work, we demonstrate that PEO is miscible with P(2EO-MO) in the neat, salt-free, state. We have also identified a range of salt concentrations over which PEO/ P(2EO-MO)/LiTFSI blends remain miscible. We use the term conventional polymer electrolytes to refer to binary mixtures of a polymer and a salt such as PEO/LiTFSI or P(2EO-MO)/ LiTFSI. We use the term polymer blend electrolyte to refer to ternary mixtures of two distinct polymers and a salt. The thermodynamic properties of PEO/P(2EO-MO)/LiTFSI were determined by small-angle neutron scattering (SANS) experiments. The SANS results are consistent with phase behavior inferences based on differential scanning calorimetry (DSC) experiments. Ion transport in the polymer blend electrolytes is compared with that obtained from conventional polymer electrolytes (PEO/LiTFSI and P(2EO-MO)/LiTFSI) by using both blocking and nonblocking electrodes.

MATERIALS AND METHODS

Synthesis of 1,3,6-Trioxocane, (2EO-MO). Diethylene glycol (100 g, 0.942 mol), paraformaldehyde (37 g, 1.3 equiv), poly-(phosphoric acid) (4.0 g, 0.03 equiv), and heptane (160 mL) were combined in a 250 mL flask fitted with a Dean-Stark adapter and condenser. The reaction was stirred at 115 °C for 12 h, and water (~15 mL) was collected as the bottom layer in the trap. After the reaction mixture was cooled to room temperature, heptane was removed via rotary evaporation to give a cloudy, viscous solution. This oligomerized product was distilled at 150-180 °C under high vacuum into a receiving flask cooled in a dry ice/acetone bath. The crude mixture of diethylene glycol and 1,3,6-trioxocane was then fractionally distilled under high vacuum at 80 °C to give clear, colorless 1,3,6-trioxocane in 70% yield. The monomer was dried over CaH2 for 3 days, distilled, and degassed via three freeze-pump-thaw cycles. Spectral data matched that previously reported in ref 9. ¹H NMR (500 MHz, CDCl₃): δ 4.57 (s, 2H), 3.50 (s, 8H) ppm. ¹³C NMR (125 MHz, CDCl₃): δ 97.91, 72.58, 70.61 ppm. HRMS (DART-MS): m/z calculated for $C_5H_{10}O_3$ [H]⁺ 119.0703; found

Synthesis of Poly(1,3,6-trioxocane), P(2EO-MO). In a glove-box under a N_2 atmosphere, 1,3,6-trioxocane (6.0 g, 51 mmol) and CH_2Cl_2 (25.4 mL) were combined in a 100 mL flask equipped with a

Table 1. Molar Masses and Dispersities of Homopolymers Used in This Study

polymer	$M_{\rm n}~({\rm kg~mol}^{-1})$	Đ
PEO	35.0	1.08
dPEO	35.0	1.09
P(2EO-MO) sample 1	26.1	1.83
P(2EO-MO) sample 2	26.7	1.66
P(2EO-MO) sample 3	16.0	1.76
P(2EO-MO) sample 4	55.2	1.97

Table 2. Polymer Components of Blends Used in Each Experiment

experiment	component 1	component 2
DSC and electrochemistry	PEO	P(2EO-MO) sample 1
SANS	dPEO	P(2EO-MO) sample 2
SANS	dPEO	P(2EO-MO) sample 3

stir bar. Then, BF3:OEt2 (0.130 mL, 0.02 equiv) was added instantaneously, and the flask was sealed with a rubber septum. The reaction gelled after 30 min such that stirring ceased, and the solution gradually turned pink. After 1 h, the reaction was removed from the glovebox and quenched with a 1:1 mixture of acetonitrile:water (40 mL) to give a clear, colorless solution. The crude mixture was extracted with CH₂Cl₂ (30 mL × 3), dried with Na₂SO₄, filtered, and rotovapped until reaching a total volume of ~30 mL. The polymer was then precipitated into hexanes (400 mL), redissolved in CH₂Cl₂ (30 mL), and precipitated again into cold isopropanol (400 mL) to give a white solid. The polymer was dried under high vacuum overnight. Typical yields ranged from 50 to 60%, and ¹H and ¹³C NMR analyses suggest that the polymerization proceeds with excellent regioregularity. Notably, polymerization is initiated by adventitious water in the reaction mixture. Furthermore, monomer conversion is highly dependent on monomer concentration and reaction temperature. Therefore, molar mass is difficult to control in this system, and variance was expected across multiple batches. Sample 1: $M_n = 26.1 \text{ kg mol}^{-1}$, D = 1.83. Sample 2: $M_n = 16.1 \text{ kg}$ mol^{-1} , $\mathcal{D} = 1.76$. Sample 3: $M_{\text{n}} = 26.7 \text{ kg mol}^{-1}$, $\mathcal{D} = 1.66$. Sample 4: $M_{\rm n} = 55.2 \text{ kg mol}^{-1}$, D = 1.97. $T_{\rm g} = -66 \,^{\circ}\text{C}$, $T_{\rm m} = 39 \,^{\circ}\text{C}$. Spectral data matched that previously reported in ref 9. ^{1}H NMR (500 MHz, CDCl₃): δ 4.74 (s, 2H), 3.69 (m, 8H) ppm. ¹³C NMR (125 MHz, CDCl₃): δ 95.73, 70.60, 67.02 ppm.

Polymer Blend Electrolyte Preparation and Composition. The molar masses, $M_{\rm n}$, and dispersities, D, of PEO (Polymer Source), deuterated PEO (dPEO) (Polymer Source), and P(2EO-MO) (synthesized as described above) used in this study are summarized in Table 1.

Electrolytes used for SANS experiments were made up of blends of dPEO, P(2EO-MO) ($M_{\rm n}=26.7~{\rm or}~16.0~{\rm kg~mol^{-1}}$), and LiTFSI, while electrolytes for DSC and electrochemical experiments were made up of blends of PEO, P(2EO-MO) ($M_{\rm n}=26.1~{\rm kg~mol^{-1}}$), and LiTFSI (see Table 2). Electrochemical measurements were also performed on conventional polymer electrolytes of P(2EO-MO) ($M_{\rm n}=55.2~{\rm kg~mol^{-1}}$) with LiTFSI. All polymers were dried in a glovebox antechamber under vacuum at 90 °C for at least 24 h prior to use. LiTFSI was dried under vacuum at 120 °C for at least 72 h.

The polymer composition of the blends was 50/50 by weight. We denote component 1 as PEO and component 2 as P(2EO-MO). The volume fraction of each component, on a salt-free basis, is given by

$$\phi_1 = \frac{\frac{w_1}{\rho_1}}{\frac{w_1}{\rho_1} + \frac{w_2}{\rho_2}} \tag{1}$$

and

$$\phi_2 = 1 - \phi_1 \tag{2}$$

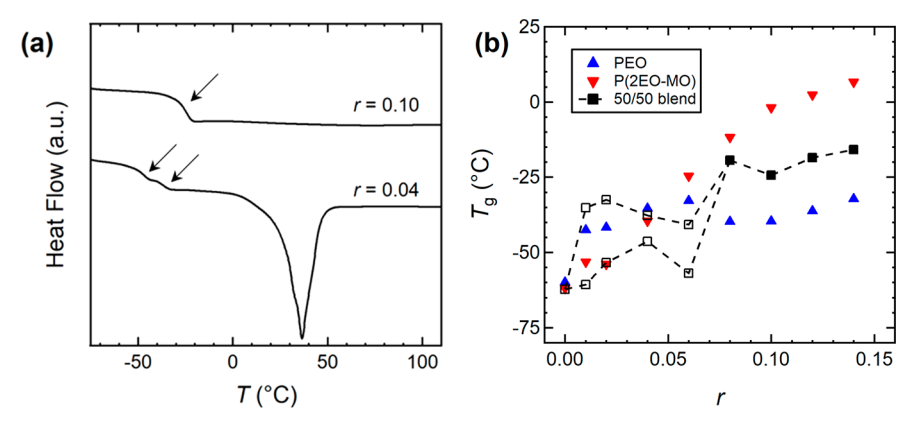


Figure 2. (a) Representative DSC curves showing one $T_{\rm g}$ for a 50/50 blend of PEO ($M_{\rm n}=35.0~{\rm kg~mol^{-1}}$) and P(2EO-MO) ($M_{\rm n}=26.1~{\rm kg~mol^{-1}}$) at r=0.10 and two $T_{\rm g}$ values at r=0.04. Arrows denote regions associated with the glass transition. (b) $T_{\rm g}$ as a function of salt concentration, r, for each conventional polymer electrolyte system (solid blue triangles for PEO ($M_{\rm n}=100~{\rm kg~mol^{-1}}$) and solid red triangles for P(2EO-MO) ($M_{\rm n}=55.2~{\rm kg~mol^{-1}}$)) and the polymer blend electrolytes. Polymer blends possessing a single $T_{\rm g}$ at high r values ($0.08 \le r \le 0.14$) and blends exhibiting two $T_{\rm g}$ values at low r values ($0.02 \le r \le 0.06$) are denoted by closed black squares and open black squares, respectively. The uncertainty of the $T_{\rm g}$ measurements is assumed to be that of the instrument's given calorimetric reproducibility and precision ($\pm 0.05\%$). Data for PEO and P(2EO-MO) were taken from ref 9.

where w_i and ρ_i are the mass and density, respectively, of component i in the blend. The volume fractions are approximately equal (see Table 3). The volume fraction occupied by the polymer components in the blends containing LiTFSI is given by

$$\phi_{\text{polymer}} = \frac{\frac{w_1}{\rho_1} + \frac{w_2}{\rho_2}}{\frac{w_1}{\rho_1} + \frac{w_2}{\rho_2} + \frac{w_{\text{salt}}}{\rho_{\text{salt}}}}$$
(3)

where $w_{\rm salt}$ is the mass of LiTFSI in the blend and $\rho_{\rm salt} = 2.023$ g cm^{-3.11} Volume changes of mixing are ignored in our analysis.

We assume that the salt is uniformly distributed in the blend. The salt concentration of the blends was quantified by the molar ratio of Li atoms in the salt to O atoms in the polymers (r = [Li]/[O]), calculated as follows:

$$r = \frac{\frac{\frac{w_{\text{salt}}}{M_{\text{salt}}}}{\frac{w_1}{M_{\text{EO}}} + \frac{3w_2}{M_{\text{2EO-MO}}}}$$
(4)

where $M_{\rm EO}$ is the monomer molar mass of PEO ($M_{\rm EO}=44.05~{\rm g}~{\rm mol}^{-1}$), $M_{\rm 2EO-MO}$ is the monomer molar mass of P(2EO-MO) ($M_{\rm 2EO-MO}=118.1~{\rm g}~{\rm mol}^{-1}$), and $M_{\rm salt}$ is the molar mass of LiTFSI ($M_{\rm salt}=287.1~{\rm g}~{\rm mol}^{-1}$). A factor of 3 was included as 2EO-MO contains three oxygen atoms, while EO contains one oxygen atom per monomer, as shown in Figure 1.

The volume fraction of PEO and the LiTFSI associated with PEO in the polymer blend electrolytes, f, is estimated via the following equation:

$$f = \frac{\frac{w_1 + \frac{rw_1 M_{\text{salt}}}{M_1}}{\rho_1}}{\frac{w_1 + \frac{rw_1 M_{\text{salt}}}{M_1}}{\rho_1} + \frac{w_2 + \frac{3rw_2 M_{\text{salt}}}{M_2}}{\rho_2}}$$
(5)

Equation 5 is based on the assumption that the value of r in the PEO-rich fluctuations is the same as that in the P(2EO-MO)-rich fluctuations.

Electrolyte r values ranged from 0 to 0.14. All electrolyte solutions in acetonitrile were transparent, indicating complete dispersion of all mixture components. The electrolytes were stirred on a hot plate at 80 °C until all of the acetonitrile had evaporated and then further dried in a glovebox antechamber under vacuum at 90 °C for 24 h to remove any residual solvent.

Density measurements for neat P(2EO-MO) at 90 °C were taken by measuring the mass of electrolyte within a known volume, following procedures described previously. The average of three density measurements (ρ_2 = 1.32 \pm 0.04 g cm⁻³) was used for subsequent calculations.

DSC Sample Preparation and Experiments. Samples (\sim 10 mg) were hermetically sealed in aluminum pans in an argon glovebox. DSC experiments were run with two heating and cooling cycles at a heating rate of 20 °C min⁻¹ and a cooling rate of 5 °C min⁻¹ using a Thermal Advantage Q200 calorimeter at the Molecular Foundry, Lawrence Berkeley National Lab. The temperature ranged from -80 to 120 °C. The glass transition temperature ($T_{\rm g}$) values are obtained from analysis of the second heating run.

SANS Sample Preparation and Experiment. Sample preparation for SANS experiments was conducted following procedures outlined previously. The blends were made such that the volume fractions of each component were ~ 0.5 (see Table 3).

SANS experiments were conducted on the NG7SANS beamline at the National Institute of Standards and Technology Center for Neutron Research.¹³ Measurements were performed with a neutron wavelength of 6 Å and up to three sample-to-detector distances (SDDs) of 13, 4, and 1 m. The shortest, 1 m distance, was used with a detector offset of 25 cm to extend the scattering angle (2θ) attainable. Overall, the three configurations allowed for access to a scattering wave-vector magnitude, $q = \frac{4\pi}{\lambda} \sin(\theta)$, ranging from 0.03 to 5.5 nm⁻¹. The neutron beam size was defined by a 9.5×10^{-3} m aperture. Data were collected at 10 °C increments between 60 and 110 °C. All measurements were reversible and repeatable upon either heating or cooling. Samples were equilibrated for at least 30 min at each temperature. A 9-position Peltier cooling/heating sample changer block was used to drive and maintain constant sample temperature. Samples of thickness of 1 mm were used. Data were reduced by using the software package for IGOR provided by the NIST Center for Neutron Research. 14 The total scattering intensity was corrected for detector sensitivity, background, and empty cell contributions as well as sample transmission and thickness. 14,15

Electrochemical Sample Preparation and Experiments. Electrochemical sample preparation and experiments were conducted following the procedures previously described, 16 using 508 μ m thick silicone spacers and conducting the measurements at 90 °C.

RESULTS AND DISCUSSION

A commonly used method to determine polymer miscibility is the measurement of the glass transition temperature, $T_{\rm g}$, via DSC. The existence of a single $T_{\rm g}$ is indicative of a miscible

blend. Figure 2a shows DSC curves for PEO/P(2EO-MO)/LiTFSI blends at r=0.04 and 0.10. The r=0.04 blend exhibits two glass transitions ($T_{\rm g1}=-46~{}^{\circ}{\rm C}$, $T_{\rm g2}=-38~{}^{\circ}{\rm C}$) which indicates the blend is phase separated. In contrast, the r=0.10 blend exhibits a single glass transition ($T_{\rm g}=-24~{}^{\circ}{\rm C}$), which indicates that the blend is composed of a single phase. The absence of a melting transition in the DSC data from the higher salt blend is consistent with numerous reports in the literature indicating that the addition of salt suppresses crystallization of PEO. P.16,18,19 All of the thermodynamic and electrochemical data presented in this paper were obtained above the melting temperatures of the blends.

Figure 2b shows the complete set of glass transition temperatures for each polymer blend electrolyte and the corresponding conventional polymer electrolyte taken from ref 9. In the neat blend, the $T_{\rm g}$ values of PEO and P(2EO-MO) are too close to be distinguished by DSC. For r values between 0.02 and 0.06, the polymer blend electrolytes exhibit two $T_{\rm g}$ values, denoted by open squares, indicating immiscibility. However, from r=0.08 to 0.14, the blend has a single $T_{\rm g}$ indicating miscibility at these higher salt concentrations. The $T_{\rm g}$ for all systems generally increases with increasing salt concentration. The correlation between $T_{\rm g}$ and salt loading is attributed to the solvated ions inducing physical cross-linking of the polymer chains.

The measured absolute SANS intensity, I(q), as a function of the magnitude of the scattering vector, q, for the dPEO/P(2EO-MO)/LiTFSI blends at 90 °C is shown in Figure 3.

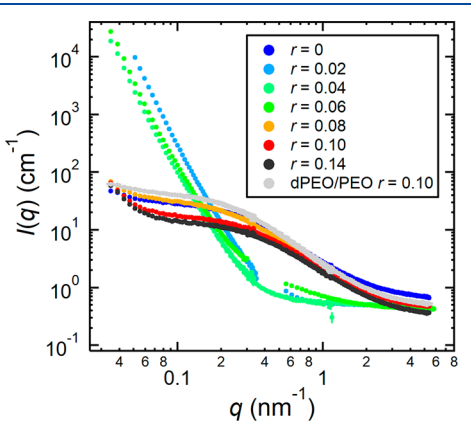


Figure 3. Measured absolute SANS intensity, I(q), vs scattering vector, q, at 90 °C, for blends of dPEO ($M_{\rm n}=35.0~{\rm kg~mol^{-1}}$) and P(2EO-MO) ($M_{\rm n}=26.7~{\rm kg~mol^{-1}}$) at varying LiTFSI salt concentrations, r, and a dPEO/PEO sample with r=0.10. Note that for r=0.02 and r=0.06 there is an intermediate range of q that was not recorded due to insufficient beamtime. Error bars represent one standard deviation of the scattering data and in most cases are smaller than the data points.

Also shown as a reference is a dPEO/PEO/LiTFSI blend with volume fraction $\phi_1=0.50$ and r=0.10 at 90 °C. Distinct differences are apparent between the scattering profiles of dPEO/P(2EO-MO)/LiTFSI blends with low salt concentrations $(0.02 \le r \le 0.06)$ and that of the neat blend (r=0) and blends with high salt concentrations $(r \ge 0.08)$. The blends with low salt concentration show a rapid rise in I(q) at low q ($q < 0.1 \text{ nm}^{-1}$), indicative of phase separation. The neat blend and high r-value blends have similar scattering profiles as that of the dPEO/PEO/LiTFSI sample. In the range 0.4 < q (nm $^{-1}$) < 2, I(q) from these blends is approximately

proportional to q^{-2} while I(q) is a much weaker function of q for q < 0.4 nm⁻¹. These features are characteristic of scattering from a homogeneous binary polymer blend wherein the polymer chains obey random walk statistics.²¹ The SANS results regarding polymer blend miscibility are consistent with the results obtained from DSC.

Analysis of SANS data begins with a thermodynamic model for the polymer blend electrolytes. We start with the thermodynamics of mixing in a two-component polymer blend in the absence of salt. The Gibbs free energy of mixing of a homogeneous mixture of two polymers can be described by the Flory—Huggins theory:

$$v\frac{\Delta G_{\rm m}}{k_{\rm B}T} = \frac{\phi_1 \ln \phi_1}{N_1} + \frac{\phi_2 \ln \phi_2}{N_2} + \chi \phi_1 \phi_2 \tag{6}$$

where $\Delta G_{\rm m}$ is the free energy of mixing per unit volume, $k_{\rm B}$ is the Boltzmann constant, T is the absolute temperature, ϕ_i is the volume fraction of component i, N_i is the number of repeat units in chain i, and χ is the Flory–Huggins interaction parameter which describes the thermodynamic incompatibility between component 1 and 2. 22,23 N_1 , N_2 , and χ are based on a reference volume, $\nu=0.1$ nm³. A miscible blend, one that is homogeneous down to the molecular level, requires both a negative Gibbs free energy of mixing ($\Delta G_{\rm m} < 0$) and a positive second derivative ($\partial^2 \Delta G_{\rm m}/\partial \phi_1^2 > 0$). The critical Flory–Huggins interaction parameter value, $\chi_{\rm crit}$ is given by the following:

$$\chi_{\text{crit}} = \frac{1}{2} \left(\frac{1}{\sqrt{N_1}} + \frac{1}{\sqrt{N_2}} \right)^2$$
(7)

Blends with $\chi < \chi_{crit}$ are predicted to be miscible, regardless of composition.

For salt-containing mixtures, we use a simple extension of eq 6:

$$v \frac{\Delta G_{\rm m}}{k_{\rm B}T} = \phi_{\rm polymer} \left(\frac{\phi_1 \ln \phi_1}{N_1} + \frac{\phi_2 \ln \phi_2}{N_2} + \chi_{\rm eff} \phi_1 \phi_2 \right) \tag{8}$$

where ϕ_{polymer} is the total polymer volume fraction and ϕ_i (i=1 or 2) are the salt-free polymer volume fractions. The effect of added salt is captured mainly by an effective Flory–Huggins parameter, χ_{eff} which depends on salt concentration. In the limit of $r \to 0$, $\phi_{\mathrm{polymer}} \to 1$, eq 8 reduces to eq 6, and χ_{eff} reduces to the conventional χ parameter for polymer blends.

Following the analysis in ref 24, the absolute SANS intensity was corrected for the contributions from scattering of the deuterated chains as well as the contributions from the incoherent scattering to obtain the absolute coherent SANS intensity:

$$I_{\text{coh}}(q) = I(q) - fI_{\text{dPEO/LiTFSI}}(q) - I_{\text{inc}}(q)$$
(9)

where f is the estimated volume fraction of dPEO and LiTFSI in our polymer blend electrolytes ($f \approx 0.5$) and $I_{\rm dPEO/LiTFSI}(q)$ is the scattering from dPEO/LiTFSI mixtures taken from ref 12. $I_{\rm inc}(q)$ is the incoherent scattering background contribution to the intensities, determined by fitting I(q) to the following expression:

$$I(q) = aP(q) + b (10)$$

where P(q) is a form factor given by the Debye function (see eq 14), a is a constant scaling factor, and b is a constant

assumed to be equal to $I_{\rm inc}(q)$. Figure 4 shows the coherent SANS profiles, $I_{\rm coh}(q)$, of the miscible blends at 90 °C.

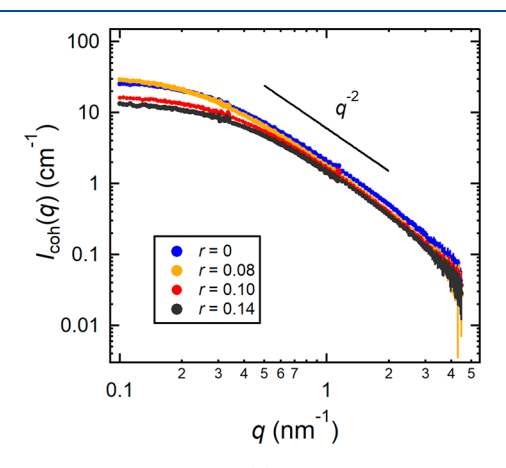


Figure 4. SANS intensities, $I_{\rm coh}(q)$, plotted as a function of the magnitude of the scattering vector, q, at 90 °C for the dPEO/P(2EO-MO)/LiTFSI (P(2EO-MO) $M_{\rm n}=26.7~{\rm kg~mol}^{-1}$) blends at the miscible salt concentrations. Error bars represent one standard deviation of the scattering data and in most cases are smaller than the data points.

The coherent scattering intensity for homogeneous PEO/P(2EO-MO)/LiTFSI blends is calculated by using the random phase approximation (RPA):

$$I_{\text{coh}}(q) = \phi_{\text{polymer}} (B_1 - B_2)^2 \nu \left(\frac{1}{S_{11}} + \frac{1}{S_{22}} - 2\chi_{\text{eff}} \right)^{-1}$$
 (11)

In our analysis, component 1 is dPEO, component 2 is P(2EO-MO), $\phi_{
m polymer}$ is the volume fraction of both polymer components, dPEO and P(2EO-MO), B_i is the coherent neutron scattering length density of component i given by B_i = b_i/ν_i , ν_i and b_i are the molar monomer volumes and neutron scattering lengths of component i, respectively, and $\chi_{\rm eff}$ is the effective Flory—Huggins interaction parameter between dPEO and P(2EO-MO) both with and without salt.^{21,24,26–28} In the limit $q \rightarrow 0$, eq 11 is consistent with eq 8. The neutron scattering lengths of dPEO and P(2EO-MO) are 4.58×10^{-12} cm and 1.32×10^{-12} cm, respectively. The molar monomer volumes of dPEO and P(2EO-MO) were calculated in the absence of salt ($\nu_1 = 38.98 \text{ cm}^3 \text{ mol}^{-1} \text{ and } \nu_2 = 89.47 \text{ cm}^3$ mol⁻¹ at 90 °C). We assume dPEO occupies the same molar volume as hydrogenous PEO. We thus obtain $\rho_1 = 1.23 \text{ g cm}^{-3}$ and $\rho_2 = 1.32 \text{ g cm}^{-3}$ at 90 °C. The temperature dependence of monomer volumes was applied to the contrast terms, and was determined by using the following equations: $\rho_1 = 1.23$ – $7.31 \times 10^{-4} (T - 363) \text{ g cm}^{-3} \text{ and } \rho_2 = 1.32 - 7.31 \times 10^{-4} (T - 363) \text{ g cm}^{-3}$

-363) g cm⁻³ where *T* is the temperature in Kelvin.²⁹ The thermal expansion coefficient of P(2EO-MO) has not been measured; it was assumed to be the same as that of PEO.

The structure factor, S_{ii} is given by

$$S_{ii} = \phi_i N_i P_i(q) \tag{12}$$

where ϕ_i is the volume fraction of polymer i on a salt-free basis. $I_{\rm coh}(q)$ depends on three volume fractions: ϕ_1 , ϕ_2 , and $\phi_{\rm polymer}$ (see eqs 11 and 12). For the blends covered in this study, these volume fractions are listed in Table 3.

 N_i is the number of repeat units in each polymer calculated by

$$N_i = \frac{M_i}{\rho_i N_{\rm av} \nu} \tag{13}$$

where $N_{\rm av}$ is Avogadro's number and M_i and ρ_i are the polymer molar masses (g mol⁻¹) and densities (g cm⁻³) of component i, and

$$P_{i}(q) = 2 \left[\frac{\exp(-x_{i}) - 1 + x_{i}}{x_{i}^{2}} \right]$$
(14)

with $x_i = q^2 R_{g,i}^2$. Both components are modeled as flexible Gaussian chains according to

$$R_{g,i}^{2} = \frac{N_{i}l_{i}^{2}}{6} \tag{15}$$

where l_i is the statistical segment length of each component. The statistical segment length of PEO is $l_1=0.58$ nm (based on a 0.1 nm³ reference volume). The statistical segment length of P(2EO-MO) has not been measured. In our calculations, we assume $l_1=l_2=l=0.58\alpha$ nm, where α is a fitting parameter that accounts for differences in the statistical segment length of PEO and P(2EO-MO) and distortions of chains (e.g., chain stretching) in the blends.

 $I_{\mathrm{coh}}(q)$ values for the miscible blends were first fit to eq 11 with two adjustable parameters: α and χ_{eff} . For each blend, α was found to be essentially invariant with temperature so α was averaged across all temperatures and fixed. The parameter α is greater than 1 for all blends, likely due to the increased stiffness of P(2EO-MO) chains relative to that of the PEO chains. These values are given in Table 3. $I_{\mathrm{coh}}(q)$ was then fit to eq 11 with only χ_{eff} as a fitting parameter. Representative RPA fits of $I_{\mathrm{coh}}(q)$ for a dPEO/P(2EO-MO) blend with r=0.08 are shown in Figure 5. χ_{eff} values of -4.67×10^{-3} and 7.64×10^{-4} are obtained from the profiles at 70 °C and 90 °C, respectively. At 110 °C, the blend is phase separated and cannot be analyzed by RPA. Note that χ_{eff} increases with increasing temperature.

Effective Flory-Huggins interaction parameters were extracted by fitting $I_{coh}(q)$ to RPA for all miscible blends

Table 3. Volume Fractions, ϕ_i , and α Values Used in RPA Fits of dPEO/P(2EO-MO)/LiTFSI Blends^a

	dPEO/P(2EO-MO)/LiTFSI (dPEO $M_{\rm n}$ = 35.0 kg mol ⁻¹ ; P(2EO-MO) $M_{\rm n}$ = 26.7 kg mol ⁻¹)				dPEO/P(2EO-MO)/LiTFSI (dPEO $M_{\rm n}$ = 35.0 kg mol ⁻¹ ; P(2EO-MO $M_{\rm n}$ = 16.0 kg mol ⁻¹)			kg mol ⁻¹ ; P(2EO-MO)
r	ϕ_1	ϕ_2	$\phi_{ ext{polymer}}$	α	ϕ_1	ϕ_2	$\phi_{ ext{polymer}}$	α
0	0.516	0.484	1	1.274 ± 0.007	0.517	0.483	1	1.331 ± 0.044
0.08	0.517	0.483	0.742	1.205 ± 0.014				
0.10	0.518	0.482	0.696	1.173 ± 0.001	0.517	0.483	0.705	1.212 ± 0.011
0.14	0.515	0.485	0.621	1.122 ± 0.002				

^aThe errors shown correspond to one standard deviation from the temperature averaging.

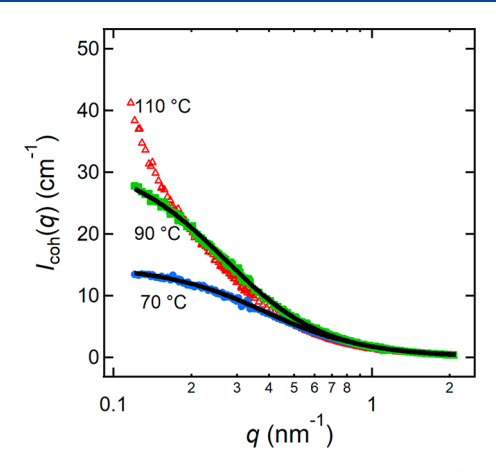


Figure 5. RPA fits (solid black lines) for a dPEO/P(2EO-MO)/LiTFSI (P(2EO-MO) $M_{\rm n} = 26.7~{\rm kg~mol}^{-1}$) blend with r = 0.08 at 70 °C (filled blue circles) and 90 °C (filled green squares). The 110 °C measurements (open red triangles) indicate phase separation. Error bars represent one standard deviation of the scattering data and in most cases are smaller than the data points.

across a range of temperatures ($60 \le T$ (°C) ≤ 110) for the high molar mass P(2EO-MO)-containing ($M_n = 26.7$ kg mol⁻¹) blends at r = 0, 0.08, 0.10, and 0.14 and the low molar mass P(2EO-MO)-containing ($M_n = 16.0$ kg mol⁻¹) blends at r = 0 and 0.10. The temperature dependence of $\chi_{\rm eff}$ is given by

$$\chi_{\text{eff}} = \frac{A}{T} + B \tag{16}$$

where A and B are empirically determined constants.^{3,30} For each blend sample, χ_{eff} was linearly fit to inverse temperature using eq 16 to extract values for A and B. These values are summarized in Table 4.

All $\chi_{\rm eff}$ parameters calculated in this study and their temperature and molar mass dependence are shown in Figure 6. Solid markers represent experimental measurements, and the solid lines are a fit to the data according to eq 16. The dashed line denotes χ_{crit} , which was calculated from eqs 7 and 13 for blends comprising P(2EO-MO) of lower (16.0 kg mol⁻¹) and higher (26.7 kg mol⁻¹) molar masses. Figure 6a shows the temperature dependence of $\chi_{\rm eff}$ in the higher molar mass P(2EO-MO)-containing blends. In the neat state, $\chi_{\rm eff}$ is negative with a value of -3.07×10^{-3} at 60 °C and increases with increasing temperature (A = -5.401), increasing to a value of -9.67×10^{-4} at 110 °C. $\chi_{\rm eff}$ is a more sensitive function of temperature in the salt-containing blends where $0.08 \le r \le 0.10$. For the r = 0.08 blend, $\chi_{\rm eff}$ increases from -4.67×10^{-3} at 70 °C to 2.77 × 10⁻³ at 100 °C, and phase separation is observed experimentally at 110 °C (see Figure 5). At 110 °C, $\chi_{\rm eff}$ predicted by extrapolating the data below 100

°C is larger than $\chi_{\rm crit} = 5.06 \times 10^{-3}$, as expected. For r = 0.10, we see a similarly strong dependence with temperature, and $\chi_{\rm eff}$ varies from -7.29×10^{-3} at 60 °C to -3.41×10^{-4} at 110 °C. The value of A is negative and B is positive for all miscible blends except at r = 0.14. At this concentration, A is positive and B is negative, and there is a very weak dependence on temperature.

Similarly, Figure 6b shows the temperature dependence of $\chi_{\rm eff}$ in the lower molar mass P(2EO-MO)-containing blends. At the same salt concentration, the temperature dependences of $\chi_{\rm eff}$ obtained from lower and higher molar mass P(2EO-MO) blends are similar. At r=0, the difference in A and B values is less than 10%, while at r=0.10, A is within 10% while the value of B differs by about 20% (see Table 4). The absolute value of $\chi_{\rm eff}$ is greater in the lower molar mass P(2EO-MO)-containing blends than in the higher molar mass blends. $\chi_{\rm eff}$ is always below $\chi_{\rm crit}=6.78\times 10^{-3}$ for these lower molar mass blends.

In all cases where $\chi_{\rm eff}$ is a sensitive function of temperature, R^2 values for the linear fits are greater than 0.98 (see Table 4). The R^2 value for the r=0.14 blend is 0.344, which is expected as $\chi_{\rm eff}$ is insensitive to temperature in this case.

Salt concentration is known to affect χ_{eff} in multicomponent polymer systems.^{31,32} This effect has primarily been studied in phase-separated or microphase-separated systems, e.g., polystyrene and PEO. $^{33-42}$ In the dPEO/P(2EO-MO) ($M_{\rm n}=26.7$ kg mol⁻¹) blend, the addition of salt up to r = 0.02 induces phase separation, while sufficient salt concentrations ($r \ge 0.08$) render the mixture miscible again. The dependence of $\chi_{\rm eff}$ on r is shown in Figure 7 for three temperatures (70 °C, 90 °C, and 110 °C). $\chi_{\rm eff}$ is slightly negative in the neat blend, with similar values across the three temperatures. Addition of salt to r =0.02 increases $\chi_{\rm eff}$ above $\chi_{\rm crit} = 5.06 \times 10^{-3}$. χ remains above this critical value at r = 0.04 and r = 0.06. Because the samples at $0.02 \le r \le 0.06$ were immiscible at all temperatures studied, no information about χ_{eff} is available besides a lower bound, as indicated in Figure 7. At 90 °C and 110 °C, $\chi_{\rm eff}$ decreases with increasing r for $r \ge 0.08$. The data in Figure 7 suggest that χ_{eff} goes through a maximum at a value of r between 0.02 and 0.08 at 90 °C and 110 °C. At 70 °C, $\chi_{\rm eff}$ is a nonmonotonic function of r for $r \ge 0.08$. At this temperature, χ_{eff} exhibits both a maximum and a minimum with respect to r.

We now discuss the ion transport properties of the higher molar mass polymer blend electrolytes. For reference, we also include ion transport properties of conventional PEO/LiTFSI ($M_n = 35.0 \text{ kg mol}^{-1}$) and P(2EO-MO)/LiTFSI ($M_n = 55.2 \text{ kg mol}^{-1}$) electrolytes.⁴³ The ionic conductivity of the PEO/P(2EO-MO)/LiTFSI blend as a function of r is shown in Figure 8a. The conductivity increases with increasing r due to the higher concentration of charge carrying species. To a good

Table 4. A and B Constants for dPEO/P(2EO-MO)/LiTFSI Blends at Various Salt Concentrations, r, and Their Linear Fit R^2 Values^a

	dPEO/P(2EO-MO)/Li	TFSI (P(2EO-MO) $M_{\rm n} = 26.$	7 kg mol ⁻¹)	dPEO/P(2EO-MO)/LiT	TFSI (P(2EO-MO) $M_{\rm n} = 16$	6.0 kg mol ⁻¹)
r	A	В	R^2	A	В	R^2
0	-5.401 ± 0.241	0.0133 ± 0.0007	0.986	-5.773 ± 0.172	0.0149 ± 0.0005	0.994
0.08	-32.127 ± 1.146	0.0891 ± 0.0032	0.997			
0.10	-17.682 ± 0.305	0.0460 ± 0.0008	0.998	-21.537 ± 0.480	0.0576 ± 0.0013	0.997
0.14	1.383 ± 1.350	-0.0072 ± 0.0037	0.344			

^aThe errors shown represent one standard deviation of uncertainty for the fit for A and B according to eq 16.

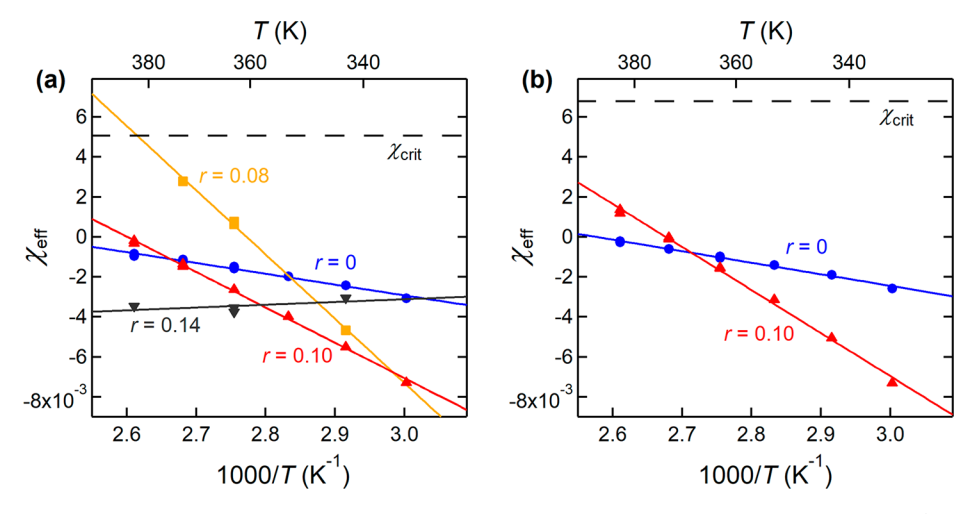


Figure 6. Effective Flory—Huggins interaction parameter, $\chi_{\rm eff}$ as a function of inverse temperature, 1/T, for the dPEO/P(2EO-MO)/LiTFSI blend (a) with higher P(2EO-MO) molar mass ($M_{\rm n} = 26.7$ kg mol⁻¹) and (b) with lower P(2EO-MO) molar mass ($M_{\rm n} = 16.0$ kg mol⁻¹). The solid lines are linear fits to the data according to eq 16; values for A and B are reported in Table 4. Error bars represent one standard deviation of the $\chi_{\rm eff}$ fits and are smaller than the symbols. Typical error bars on χ range between 5 and 20%, as previously shown in ref 24.

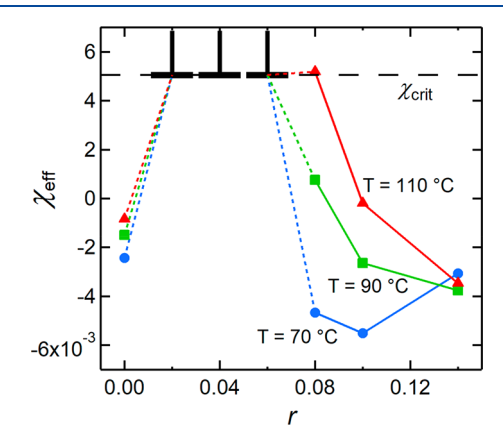


Figure 7. Effective Flory—Huggins interaction parameter, $\chi_{\rm eff}$ for the dPEO/P(2EO-MO)/LiTFSI (P(2EO-MO) $M_{\rm n}=26.7$ kg mol⁻¹) blends as a function of salt concentration, r, at three different temperatures: 70 °C (blue circles), 90 °C (green squares), and 110 °C (red triangles). The lower limit of the error bars at $0.02 \le r \le 0.06$ is the critical value for the Flory—Huggins interaction parameter, $\chi_{\rm crit}$ at which this system phase separates. Error bars for the solid markers represent one standard deviation of the $\chi_{\rm eff}$ fits and are smaller than the symbols.

approximation, the conductivity of the blend matches that of PEO/LiTFSI at all values of r.

The salt diffusion coefficient, D, of the blend shown in Figure 8b is similar to that of the conventional P(2EO-MO)/LiTFSI polymer electrolyte system for $r \leq 0.02$ but is nearly equal to that of PEO/LiTFSI for higher r. The dependence of the current fraction, ρ_+ , of the polymer blend on r, plotted in Figure 8c, matches that of PEO/LiTFSI at all salt concentrations.⁴⁴

One measure of the efficacy of an electrolyte is the product of the ionic conductivity and current fraction. This measure gives a metric for sustaining steady currents in battery applications at low current densities. The efficacies of all three electrolyte systems are similar, as shown in Figure 8d.

The immiscible blends obtained in the regime $0.01 \le r \le 0.06$ undoubtedly contain macroscopic PEO-rich and P(2EO-MO)-rich domains. However, we expect a considerable concentration of P(2EO-MO) in the PEO-rich domains, and

vice versa. The fact that the ion transport data (see Figure 8) obtained from immiscible blends do not differ significantly from that of miscible blends may be attributed to this effect. A more thorough investigation into the impact of miscibility on ion transport is warranted but is beyond the scope of this study.

We were curious whether ion transport behavior in miscible polymer blend electrolytes can be predicted based on the known properties of conventional polymer electrolytes. It is well-established that ionic conductivity in polymers depends on the relative segmental motion of the polymer backbone, which can be gauged by the $T_{\rm g}$ value. 9,19,45,46 The $T_{\rm g}$ values of the miscible polymer blend electrolytes (PEO/P(2EO-MO)/ LiTFSI) were consistently between the T_g values of the PEO/ LiTFSI and P(2EO-MO)/LiTFSI electrolytes (see Figure 2b). However, conductivity measurements indicate that PEO, the component with the lower T_g , dominates conductivity. At most salt concentrations, this general behavior also applies to the measured current fractions and salt diffusion coefficients (see Figures 8b and 8c). These observations do not indicate that only PEO chains contribute to conductivity; if this were the case, then the conductivity of the 50/50 polymer blend electrolytes would be half that of PEO/LiTFSI. The data in Figures 2b, 8b, and 8c suggest that the P(2EO-MO) chains in the miscible polymer blend electrolytes behave as if they were PEO. It is evident that ion transport in miscible polymer blend electrolytes differs qualitatively from that in conventional polymer electrolytes.

We conclude this section by reviewing previous studies of ion transport in polymer blends. It is important to distinguish between oligomers and polymers: PEO analogues such as tetraethylene glycol dimethyl ether (tetraglyme), a short chain molecule comprising four ethylene oxide units, are commonly used as solvents for electrolytic applications. The ionic conductivity of PEO/LiTFSI mixtures is independent of chain length when the molar mass of the PEO chains exceeds 2 kg mol⁻¹. The entanglement molar mass of PEO is also reported to be 2 kg mol⁻¹. This value (2 kg mol⁻¹) serves as an approximate marker to distinguish between oligomers and polymers in the context of electrolytes. There have been a few reports of mixtures of polymers, salts, and a third

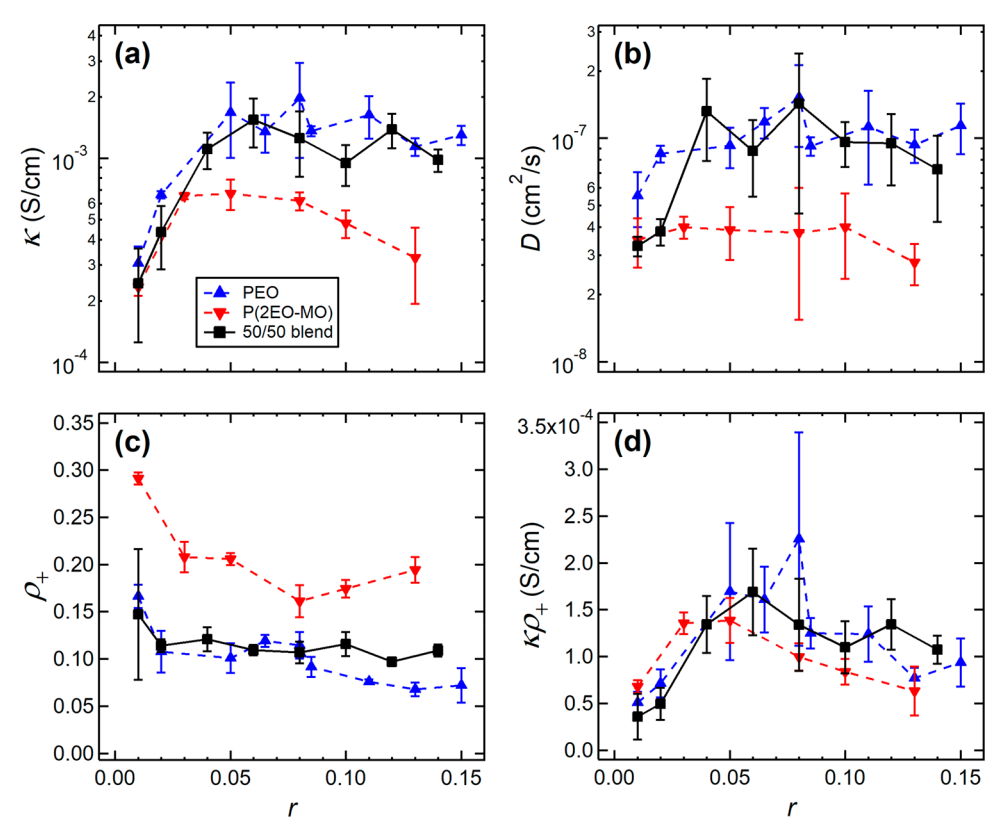


Figure 8. Electrochemical characterization of the PEO/P(2EO-MO)/LiTFSI blend as a function of salt concentration, r, compared with conventional PEO/LiTFSI ($M_n = 35.0 \text{ kg mol}^{-1}$) and P(2EO-MO)/LiTFSI ($M_n = 55.2 \text{ kg mol}^{-1}$) polymer electrolyte systems. (a) Ionic conductivity, κ , from ac impedance spectroscopy of symmetric cells with blocking electrodes. (b) Salt diffusion coefficient, D, from restricted diffusion measurements in a lithium symmetric cell. (c) Current fractions, ρ_+ , calculated from the Bruce–Vincent method using a lithium symmetric cell. (d) Efficacy, $\kappa \rho_+$. Data were taken at 90 °C. PEO/LiTFSI data were taken from ref 43. Error bars represent the standard deviation of three measurements.

component. 52-61 Tsuchida et al. studied mixtures of PEO, poly(methyl methacrylate) (PMMA), and lithium perchlorate (LiClO₄); however, the molar masses of examined PEO ranged from 0.7 to 2 kg mol⁻¹.⁵² While the miscibility of PEO and PMMA is well-established in the absence of salt, 62 the effect of added salt on miscibility is not yet known. Abraham et al. blended PEO and poly[bis((methoxyethoxy)ethoxy) phosphazene] (MEEP) with different lithium salts.⁵³ The molar mass of MEEP was not reported. Interestingly, the blends exhibited two exothermic melting transitions: one similar to that of pure PEO in the vicinity of 55 °C and an additional peak at 140 °C, in spite of the fact that MEEP is amorphous. This suggests the presence of two phases in the PEO/MEEP electrolytes. Li et al. prepared blends of PEO, poly(2-vinylpyridine) (P2VP), and LiClO₄. While PEO and P2VP are miscible in the absence of salt,⁶³ the possibility of salt-induced phase separation was not addressed. Kim et al. report both conductivity and current fraction in mixtures of PEO, poly(oligo[oxyethylene]oxysebacoyl), and LiClO₄. ⁵⁷ This is one of the few studies on electrochemical properties in polymer blends that go beyond conductivity; however, miscibility of the polymers in the presence of salt was not established. Rocco et al. studied mixtures of PEO, poly(methyl vinyl ether-maleic acid), and LiClO₄ as well as PEO, poly(bisphenol A-co-epichlorohydrin), poly(vinyl ethyl ether), and LiClO₄ blends for use as electrolytes. 59,60 Inferences regarding miscibility were mainly made on the basis of DSC. In contrast to all previous studies,52-61 this paper definitively demonstrates the miscibility of a polymer blend electrolyte system by using a rigorous approach based on SANS, wherein concentration fluctuations on the nanometer length scale are quantified. Unlike previous studies, $^{52-61}$ this work compares the characteristics of the PEO/P(2EO-MO)/LiTFSI polymer blend electrolyte system to that of its constituent polymer electrolytes (PEO/LiTFSI and P(2EO-MO)/LiTFSI).

CONCLUSION

This study demonstrates that it is possible to create homogeneous mixtures of chemically distinct polymers and a lithium salt for use in lithium batteries. This demonstration is nontrivial because polymers rarely mix with each other. Blending polymers for electrolytic applications is advantageous because of the ease of preparation and control of physical properties by simple changes in composition or chain lengths of the components. This initial study, based on PEO/P(2EO-MO)/LiTFSI, can serve as a template for future work aimed at optimizing ion transport in polymer electrolytes in a manner that mirrors the development of mixtures of organic solvents used in current day lithium ion batteries. The thermodynamic properties of PEO/P(2EO-MO)/LiTFSI blends, determined by SANS, are surprisingly complex. This initial study is restricted to blends with roughly equal volume fractions of PEO and P(2EO-MO). Neat PEO/P(2EO-MO) blends exhibit a negative Flory-Huggins interaction parameter across the accessible temperature window. If we assume that the phase behavior of PEO/P(2EO-MO)/LiTFSI blends can be

approximated by Flory–Huggins theory for binary blends of homopolymers with an effective interaction parameter that accounts for the presence of salt, it would imply that these blends would be miscible irrespective of blend composition and chain lengths of the components. Adding a small amount of LiTFSI ($0.02 \le r \le 0.06$) renders the PEO/P(2EO-MO) blends immiscible; blends containing either 26.7 or 16.0 kg mol⁻¹ P(2EO-MO) were immiscible. Increasing the salt concentration to r > 0.08 results in negative effective Flory–Huggins interaction parameters across the accessible temperature window, implying miscibility irrespective of blend composition and chain lengths of the components.

Ion transport in the blends was characterized by measuring the ionic conductivity, salt diffusion coefficient, and current fraction. Surprisingly, the values of these parameters in blends at a given salt concentration, r, were close to those obtained in conventional PEO/LiTFSI electrolytes at the same value of r. In other words, the blends that we have characterized thus far do not exhibit superior ion transport properties. However, a wide variety of ether- and carbonate-containing polymers have been synthesized for electrolytic applications. This work opens the door to a new direction for creating new and improved polymer electrolytes either by combining existing polymers with salt or by synthesizing new polymers with the specific aim of including them in miscible polymer blend electrolytes.

ASSOCIATED CONTENT

Supporting Information

The Supporting Information is available free of charge at https://pubs.acs.org/doi/10.1021/acs.macromol.0c00747.

Synthesis and characterization of P(2EO-MO) as well as ac impedance spectroscopy of representative PEO/P(2EO-MO)/LiTFSI blends (PDF)

AUTHOR INFORMATION

Corresponding Authors

Nitash P. Balsara — Department of Chemical and Biomolecular Engineering, University of California, Berkeley, Berkeley, California 94720, United States; Materials Sciences Division, Lawrence Berkeley National Laboratory, Berkeley, California 94720, United States; Joint Center for Energy Storage Research (JCESR), Argonne National Laboratory, Lemont, Illinois 60439, United States; orcid.org/0000-0002-0106-5565; Email: nbalsara@berkeley.edu

Geoffrey W. Coates — Department of Chemistry and Chemical Biology, Cornell University, Ithaca, New York 14850, United States; Joint Center for Energy Storage Research (JCESR), Argonne National Laboratory, Lemont, Illinois 60439, United States; orcid.org/0000-0002-3400-2552; Email: coates@cornell.edu

Authors

Kevin W. Gao — Department of Chemical and Biomolecular Engineering, University of California, Berkeley, Berkeley, California 94720, United States; Materials Sciences Division, Lawrence Berkeley National Laboratory, Berkeley, California 94720, United States; Joint Center for Energy Storage Research (JCESR), Argonne National Laboratory, Lemont, Illinois 60439, United States; ⊚ orcid.org/0000-0002-6794-1265

Whitney S. Loo – Department of Chemical and Biomolecular Engineering, University of California, Berkeley, Berkeley,

California 94720, United States; o orcid.org/0000-0002-9773-3571

Rachel L. Snyder — Department of Chemistry and Chemical Biology, Cornell University, Ithaca, New York 14850, United States; Joint Center for Energy Storage Research (JCESR), Argonne National Laboratory, Lemont, Illinois 60439, United States; orcid.org/0000-0002-0569-0704

Brooks A. Abel — Department of Chemistry and Chemical Biology, Cornell University, Ithaca, New York 14850, United States; Joint Center for Energy Storage Research (JCESR), Argonne National Laboratory, Lemont, Illinois 60439, United States; orcid.org/0000-0002-2288-1975

Youngwoo Choo – Materials Sciences Division, Lawrence Berkeley National Laboratory, Berkeley, California 94720, United States; Joint Center for Energy Storage Research (JCESR), Argonne National Laboratory, Lemont, Illinois 60439, United States; Oorcid.org/0000-0003-2715-0618

Andrew Lee — Department of Chemical and Biomolecular Engineering, NYU Tandon School of Engineering, New York University, Brooklyn, New York 11201, United States

Susana C. M. Teixeira — NIST Center for Neutron Research, National Institute of Standards and Technology, Gaithersburg, Maryland 20899, United States; Department of Chemical and Biomolecular Engineering, University of Delaware, Newark, Delaware 19716, United States

Bruce A. Garetz — Department of Chemical and Biomolecular Engineering, NYU Tandon School of Engineering, New York University, Brooklyn, New York 11201, United States;
ocid.org/0000-0002-3141-7840

Complete contact information is available at: https://pubs.acs.org/10.1021/acs.macromol.0c00747

Notes

The statements, findings, conclusions and recommendations are those of the authors and do not necessarily reflect the view of NIST or the U.S. Department of Commerce. Certain commercial equipment, instruments, suppliers and software are identified in this paper to foster understanding. Such identification does not imply recommendation or endorsement by the National Institute of Standards and Technology, nor does it imply that the materials or equipment identified are necessarily the best available for the purpose.

The authors declare no competing financial interest.

ACKNOWLEDGMENTS

This work was intellectually led by the Joint Center for Energy Storage Research (JCESR), an Energy Innovation Hub funded by the U.S. Department of Energy, Office of Science, Office of Basic Energy Science, under Contract DE-AC02-06CH11357, which supported synthesis work conducted by R.L.S. and B.A.A. under the supervision of G.W.C and characterization work conducted by K.W.G., W.S.L., and Y.C. under the supervision of N.P.B. Characterization work conducted by A.L. under the supervision of B.A.G. was supported by the National Science Foundation through Award DMR-1904537. Work at the Molecular Foundry, which is a DOE Office of Science User Facility, was supported by Contract DE-AC02-05CH11231. S.C.M.T. acknowledges the Center for Neutron Studies at the University of Delaware and funding under cooperative agreements #370NANB17H302 and #70NANB15H260 from NIST, U.S. Department of Commerce. We acknowledge the support of the National Institute of Standards and Technology,

U.S. Department of Commerce, in providing the neutron facilities used in this work. K.W.G. acknowledges funding from a National Defense and Science Engineering Graduate Fellowship. W.S.L. acknowledges funding from the National Science Foundation Graduate Student Research Fellowship DGE-1106400.

■ LIST OF SYMBOLS

■ LIST OF	SYMBOLS
PEO	poly(ethylene oxide)
P(2EO-MO)	poly(1,3,6-trioxocane)
LiTFSI	lithium bis(trifluoromethanesulfonyl)imide
SANS	small-angle neutron scattering
DSC	differential scanning calorimetry
2EO-MO	1,3,6-trioxocane
$M_{ m n}$	number-average molar mass (kg mol ⁻¹)
Đ	dispersity
dPEO	deuterated poly(ethylene oxide)
ϕ_i	volume fraction of component i
$\phi_{ ext{polymer}}$	volume fraction of polymer components in a
	blend containing LiTFSI
w_i	weight of component <i>i</i> (g)
$w_{ m salt}$	weight of LiTFSI salt (g)
$ ho_i$	density of component <i>i</i> (g cm ⁻³)
$ ho_{ m salt}$	density of LiTFSI salt (g cm ⁻³)
r M	molar ratio of lithium to oxygen atoms monomer molar mass of PEO (g mol ⁻¹)
$M_{ m EO}$	monomer molar mass of P(2EO-MO) (g
$M_{ m 2EO\text{-}MO}$	mol^{-1})
$M_{ m salt}$	molar mass of LiTFSI salt (g mol ⁻¹)
f salt	volume fraction of PEO and LiTFSI associated
J	with PEO
$T_{\rm g}$	glass transition temperature
SDD	sample-to-detector distance
θ	scattering angle
q	magnitude of the scattering vector (nm ⁻¹)
$\bar{\lambda}$	wavelength (nm)
q	magnitude of the scattering vector (nm ⁻¹)
I(q)	measured absolute SANS intensity (cm ⁻¹)
$\Delta G_{ m m}$	free energy of mixing per unit volume (J m ⁻³)
$k_{ m B}$	Boltzmann constant (m ² kg s ⁻² K ⁻¹)
ν	reference volume (nm³)
T	absolute temperature (K)
N_i	number of repeat units per chain
χ	Flory—Huggins interaction parameter
χ _{crit}	critical Flory—Huggins interaction parameter effective Flory—Huggins interaction parameter
$rac{\chi_{ ext{eff}}}{I_{ ext{coh}}(q)}$	coherent scattering intensity (cm ⁻¹)
$I_{\text{dPEO/LiTFSI}}(q)$	SANS intensity from dPEO/LiTFSI mixtures
-dPEO/LITFSI(4)	(cm ⁻¹)
$I_{ m inc}(q)$	incoherent scattering intensity (cm ⁻¹)
$P_i(q)$	form factor
B_i	neutron scattering length density of component
•	$i \left(\text{cm}^{-2} \text{ mol}^{-1} \right)$
b_i	neutron scattering length of component i (cm
	mol^{-1})
ν_i	monomer molar volume of component i (cm ³
	mol^{-1})
S_{ii}	structure factor
M_i	molar mass of component $i \text{ (g mol}^{-1})$
$R_{g,i}$	radius of gyration (cm)
l_i	statistical segment length of component <i>i</i> (nm)

RPA fitting parameter accounting for chain

distortion

 α

A, B	empirical constants for fitting χ
A, B R^2	coefficient of determination
κ	ionic conductivity (S cm ⁻¹)
D	salt diffusion coefficient $(cm^2 s^{-1})$
$ ho_{\scriptscriptstyle +}$	current fraction
κho_+	efficacy (S cm ⁻¹)
PMMA	poly(methyl methacrylate)
LiClO ₄	lithium perchlorate
MEEP	poly[bis((methoxyethoxy)ethoxy)-
	phosphazene]
P2VP	poly(2-vinylpyridine)

REFERENCES

- (1) Xu, K. Nonaqueous Liquid Electrolytes for Lithium-Based Rechargeable Batteries. *Chem. Rev.* **2004**, *104*, 4303–4417.
- (2) Flory, P. J. Principles of Polymer Chemistry; Cornell University Press: Ithaca, NY, 1953.
- (3) Knychała, P.; Timachova, K.; Banaszak, M.; Balsara, N. P. 50th Anniversary Perspective: Phase Behavior of Polymer Solutions and Blends. *Macromolecules* **2017**, *50* (8), 3051–3065.
- (4) Lohse, D. J. The Melt Compatibility of Blends of Polypropylene and Ethylene-propylene Copolymers. *Polym. Eng. Sci.* **1986**, *26* (21), 1500–1509.
- (5) Kwag, H.; Rana, D.; Cho, K.; Rhee, J.; Woo, T.; Lee, B. H.; Choe, S. Binary Blends of Metallocene Polyethylene with Conventional Polyolefins: Rheological and Morphological Properties. *Polym. Eng. Sci.* **2000**, *40* (7), 1672–1681.
- (6) Fenton, D. E.; Parker, J. M.; Wright, P. V. Complexes of Alkali Metal Ions with Poly(Ethylene Oxide). *Polymer* **1973**, *14* (11), 589. (7) Armand, M. Polymer Solid Electrolytes an Overview. *Solid State Ionics* **1983**, 9–10, 745–754.
- (8) Xue, Z.; He, D.; Xie, X. Poly(Ethylene Oxide)-Based Electrolytes for Lithium-Ion Batteries. *J. Mater. Chem. A* **2015**, 3 (38), 19218–19253.
- (9) Zheng, Q.; Pesko, D. M.; Savoie, B. M.; Timachova, K.; Hasan, A. L.; Smith, M. C.; Miller, T. F.; Coates, G. W.; Balsara, N. P. Optimizing Ion Transport in Polyether-Based Electrolytes for Lithium Batteries. *Macromolecules* **2018**, *51* (8), 2847–2858.
- (10) Wheatle, B. K.; Lynd, N. A.; Ganesan, V. Effect of Host Incompatibility and Polarity Contrast on Ion Transport in Ternary Polymer-Polymer-Salt Blend Electrolytes. *Macromolecules* **2020**, *53* (3), 875–884.
- (11) Pesko, D. M.; Timachova, K.; Bhattacharya, R.; Smith, M. C.; Villaluenga, I.; Newman, J.; Balsara, N. P. Negative Transference Numbers in Poly(Ethylene Oxide)-Based Electrolytes. *J. Electrochem. Soc.* **2017**, *164* (11), E3569–E3575.
- (12) Loo, W. S.; Mongcopa, K. I.; Gribble, D. A.; Faraone, A. A.; Balsara, N. P. Investigating the Effect of Added Salt on the Chain Dimensions of Poly(Ethylene Oxide) through Small-Angle Neutron Scattering. *Macromolecules* **2019**, 52 (22), 8724–8732.
- (13) Glinka, C. J.; Barker, J. G.; Hammouda, B.; Krueger, S.; Moyer, J. J.; Orts, W. J. The 30 m Small-Angle Neutron Scattering Instruments at the National Institute of Standards and Technology. *J. Appl. Crystallogr.* **1998**, *31* (3), 430–445.
- (14) Kline, S. R. Reduction and Analysis of SANS and USANS Data Using IGOR Pro. *J. Appl. Crystallogr.* **2006**, 39 (6), 895–900.
- (15) Kline, S. SANS Data Reduction Tutorial; NIST Center for Neutron Research: 2001.
- (16) Gao, K. W.; Jiang, X.; Hoffman, Z. J.; Sethi, G. K.; Chakraborty, S.; Villaluenga, I.; Balsara, N. P. Optimizing the Monomer Structure of Polyhedral Oligomeric Silsesquioxane for Ion Transport in Hybrid Organic—Inorganic Block Copolymers. *J. Polym. Sci.* **2020**, *58* (2), 363–371.
- (17) Utracki, L. A.; Wilkie, C. A. Polymer Blends Handbook, 2nd ed.; Springer: New York, 2014.
- (18) Vallée, A.; Besner, S.; Prud'Homme, J. Comparative Study of Poly(Ethylene Oxide) Electrolytes Made with LiN(CF₃SO₂)₂,

- LiCF₃SO₃ and LiClO₄: Thermal Properties and Conductivity Behaviour. *Electrochim. Acta* **1992**, 37 (9), 1579–1583.
- (19) Lascaud, S.; Perrier, M.; Vallée, A.; Besner, S.; Prud'homme, J.; Armand, M. Phase Diagrams and Conductivity Behavior of Poly-(Ethylene Oxide)-Molten Salt Rubbery Electrolytes. *Macromolecules* **1994**, 27 (25), 7469–7477.
- (20) Le Nest, J. F.; Gandini, A.; Cheradame, H.; Cohen-Addad, J. P. Influence of LiClO₄ on the Properties of Polyether Networks: Specific Volume and Glass Transition Temperature. *Macromolecules* **1988**, *21* (4), 1117–1120.
- (21) de Gennes, P. G. Scaling Concepts in Polymer Chemistry; Cornell University Press: Ithaca, NY, 1979.
- (22) Flory, P. J. Thermodynamics of High Polymer Solutions. J. Chem. Phys. 1942, 10 (1), 51–61.
- (23) Huggins, M. L. Some Properties of Solutions of Long-Chain Compounds. J. Phys. Chem. 1942, 46 (1), 151–158.
- (24) Balsara, N. P.; Fetters, L. J.; Hadjichristidis, N.; Lohse, D. J.; Han, C. C.; Graessley, W. W.; Krishnamoorti, R. Thermodynamic Interactions in Model Polyolefin Blends Obtained by Small-Angle Neutron Scattering. *Macromolecules* **1992**, *25* (23), 6137–6147.
- (25) Dubner, W. S.; Schultz, J. M.; Wignall, G. D. Estimation of Incoherent Backgrounds in SANS Studies of Polymers. *J. Appl. Crystallogr.* **1990**, 23 (6), 469–475.
- (26) de Gennes, P. G. Theory of X-Ray Scattering by Liquid Macromolecules with Heavy Atom Labels. *J. Phys.* (*Paris*) **1970**, *31* (2–3), 235–238.
- (27) Hammouda, B. Random Phase Approximation for Compressible Polymer Blends. J. Non-Cryst. Solids 1994, 172–174, 927–931.
- (28) Qiu, J.; Mongcopa, K. I.; Han, R.; López-Barrón, C. R.; Robertson, M. L.; Krishnamoorti, R. Thermodynamic Interactions in a Model Polydiene/Polyolefin Blend Based on 1,2-Polybutadiene. *Macromolecules* **2018**, *51* (8), 3107–3115.
- (29) Mark, J. E. *Physical Properties of Polymers Handbook*, 2nd ed.; Springer: New York, 2007.
- (30) Bates, F. S.; Fredrickson, G. H. Block Copolymer Thermodynamics: Theory And Experiment. *Annu. Rev. Phys. Chem.* **1990**, 41 (1), 525–557.
- (31) Wang, Z. G. Effects of Ion Solvation on the Miscibility of Binary Polymer Blends. *J. Phys. Chem. B* **2008**, *112* (50), 16205–16213.
- (32) Nakamura, I.; Balsara, N. P.; Wang, Z. G. Thermodynamics of Ion-Containing Polymer Blends and Block Copolymers. *Phys. Rev. Lett.* **2011**, *107* (19), 1–5.
- (33) Young, W. S.; Epps, T. H. Salt Doping in PEO-Containing Block Copolymers: Counterion and Concentration Effects. *Macromolecules* **2009**, 42 (7), 2672–2678.
- (34) Naidu, S.; Ahn, H.; Gong, J.; Kim, B.; Ryu, D. Y. Phase Behavior and Ionic Conductivity of Lithium Perchlorate-Doped Polystyrene-b-Poly(2-Vinylpyridine) Copolymer. *Macromolecules* **2011**, *44* (15), 6085–6093.
- (35) Huang, J.; Tong, Z. Z.; Zhou, B.; Xu, J. T.; Fan, Z. Q. Salt-Induced Microphase Separation in Poly(ε-Caprolactone)-b-Poly-(Ethylene Oxide) Block Copolymer. *Polymer* **2013**, *54* (12), 3098–3106.
- (36) Teran, A. A.; Balsara, N. P. Thermodynamics of Block Copolymers with and without Salt. *J. Phys. Chem. B* **2014**, *118* (1), 4–17.
- (37) Irwin, M. T.; Hickey, R. J.; Xie, S.; So, S.; Bates, F. S.; Lodge, T. P. Structure-Conductivity Relationships in Ordered and Disordered Salt-Doped Diblock Copolymer/Homopolymer Blends. *Macromolecules* **2016**, 49 (18), 6928–6939.
- (38) Xie, S.; Lodge, T. P. Phase Behavior of Binary Polymer Blends Doped with Salt. *Macromolecules* **2018**, *51*, 266–274.
- (39) Hou, K. J.; Qin, J. Solvation and Entropic Regimes in Ion-Containing Block Copolymers. *Macromolecules* **2018**, *51*, 7463–7475. (40) Loo, W. S.; Jiang, X.; Maslyn, J. A.; Oh, H. J.; Zhu, C.; Downing, K. H.; Balsara, N. P. Reentrant Phase Behavior and Coexistence in Asymmetric Block Copolymer Electrolytes. *Soft Matter* **2018**, *14* (15), 2789–2795.

- (41) Loo, W. S.; Balsara, N. P. Organizing Thermodynamic Data Obtained from Multicomponent Polymer Electrolytes: Salt-Containing Polymer Blends and Block Copolymers. *J. Polym. Sci., Part B: Polym. Phys.* **2019**, *57* (18), 1177–1187.
- (42) Morris, M. A.; Sung, S. H.; Ketkar, P. M.; Dura, J. A.; Nieuwendaal, R. C.; Epps, T. H. Enhanced Conductivity via Homopolymer-Rich Pathways in Block Polymer-Blended Electrolytes. *Macromolecules* **2019**, 52 (24), 9682–9692.
- (43) Gribble, D. A.; Frenck, L.; Shah, D. B.; Maslyn, J. A.; Loo, W. S.; Mongcopa, K. I. S.; Pesko, D. M.; Balsara, N. P. Comparing Experimental Measurements of Limiting Current in Polymer Electrolytes with Theoretical Predictions. *J. Electrochem. Soc.* **2019**, 166 (14), A3228–A3234.
- (44) Galluzzo, M. D.; Maslyn, J. A.; Shah, D. B.; Balsara, N. P. Ohm's Law for Ion Conduction in Lithium and beyond-Lithium Battery Electrolytes. *J. Chem. Phys.* **2019**, *151* (2), 020901.
- (45) Ratner, M. A.; Johansson, P.; Shriver, D. F. P Olymer Electrolytes: Ionic Transport Mechanisms and Relaxation Coupling. *MRS Bull.* **2000**, 25, 31–37.
- (46) Borodin, O.; Smith, G. D. Mechanism of Ion Transport in Amorphous Poly(Ethylene Oxide)/LiTFSI from Molecular Dynamics Simulations. *Macromolecules* **2006**, *39*, 1620–1629.
- (47) Jung, H.-G.; Hassoun, J.; Park, J.-B.; Sun, Y.-K.; Scrosati, B. An Improved High-Performance Lithium-Air Battery. *Nat. Chem.* **2012**, *4*, 579–585.
- (48) Nasybulin, E.; Xu, W.; Engelhard, M. H.; Nie, Z.; Burton, S. D.; Cosimbescu, L.; Gross, M. E.; Zhang, J. Effects of Electrolyte Salts on the Performance Li-O2 Batteries. *J. Phys. Chem. C* **2013**, *117*, 2635–2645.
- (49) Jache, B.; Binder, J. O.; Abe, T.; Adelhelm, P. A Comparative Study on the Impact of Different Glymes and Their Derivatives as Electrolyte Solvents for Graphite Co-Intercalation Electrodes in Lithium-Ion and Sodium-Ion Batteries. *Phys. Chem. Chem. Phys.* **2016**, 18, 14299–14316.
- (50) Teran, A. A.; Tang, M. H.; Mullin, S. A.; Balsara, N. P. Effect of Molecular Weight on Conductivity of Polymer Electrolytes. *Solid State Ionics* **2011**, 203, 18–21.
- (51) Fetters, L. J.; Lohse, D. J.; Milner, S. T.; Graessley, W. W. Packing Length Influence in Linear Polymer Melts on the Entanglement, Critical, and Reptation Molecular Weights. *Macromolecules* **1999**, 32, 6847–6851.
- (52) Tsuchida, E.; Ohno, H.; Tsunemi, K.; Kobayashi, N. Lithium Ionic Conduction in Poly(Methacrylic Acid)-Poly(Ethylene Oxide) Complex Containing Lithium Perchlorate. *Solid State Ionics* **1983**, *11*, 227–233.
- (53) Abraham, K. M.; Alamgir, M.; Reynolds, R. K. Polyphosphazene-Poly(Olefin Oxide) Mixed Polymer Electrolytes. *J. Electrochem. Soc.* **1989**, *136* (12), 3576–3582.
- (54) Orihara, K.; Yonekura, H. Nonlinear Effects on the Ionic Conductivity of Poly(Ethylene Oxide)/Lithium Perchlorate Complexes Caused by the Blending of Poly(Vinyl Acetate). *J. Macromol. Sci., Chem.* 1990, 27, 1217–1223.
- (55) Li, J.; Mintz, E. A.; Khan, I. M. Poly(Ethylene Oxide)/(Poly(2-Vinylpyridine)/Lithium Perchlorate Blends. New Materials for Solid Polymer Electrolytes. *Chem. Mater.* **1992**, *4* (6), 1131–1134.
- (56) Acosta, J. L.; Morales, E. Structural, Morphological and Electrical Characterization of Polymer Electrolytes Based on PEO/PPO Blends. *Solid State Ionics* **1996**, *85*, 85–90.
- (57) Kim, D.; Park, J.; Rhee, H. Conductivity and Thermal Studies of Solid Polymer Electrolytes Prepared by Blending Poly(Ethylene Oxide), Poly(Oligo[Oxyethylene]Oxysebacoyl) and Lithium Perchlorate. *Solid State Ionics* 1996, 83, 49–56.
- (58) Jacob, M. M. E.; Prabaharan, S. R. S.; Radhakrishna, S. Effect of PEO Addition on the Electrolytic and Thermal Properties of PVDF-LiClO4 Polymer Electrolytes. *Solid State Ionics* **1997**, *104*, 267–276.
- (59) Rocco, A. M.; da Fonseca, C. P.; Pereira, R. P. A Polymeric Solid Electrolyte Based on a Binary Blend of Poly(Ethylene Oxide), Poly(Methyl Vinyl Ether-Maleic Acid) and LiClO4. *Polymer* **2002**, *43* (13), 3601–3609.

- (60) Rocco, A. M.; de Assis Carias, A.; Pereira, R. P. Polymer Electrolytes Based on a Ternary Miscible Blend of Poly(Ethylene Oxide), Poly(Bisphenol A-Co-Epichlorohydrin) and Poly(Vinyl Ethyl Ether). *Polymer* **2010**, *51* (22), 5151–5164.
- (61) Correia, D. M.; Costa, C. M.; Nunes-Pereira, J.; Silva, M. M.; Botelho, G.; Ribelles, J.; Lanceros-Mendez, S. Physicochemical Properties of Poly(Vinylidene Fluoride-Trifluoroethylene)/Poly-(Ethylene Oxide) Blend Membranes for Lithium Ion Battery Applications: Influence of Poly(Ethylene Oxide) Molecular Weight. Solid State Ionics 2014, 268, 54–67.
- (62) Ito, H.; Russell, T. P.; Wignall, G. D. Interactions in Mixtures of Poly(Ethylene Oxide) and Poly(Methyl Methacrylate). *Macromolecules* **1987**, 20 (9), 2213–2220.
- (63) Yeh, C.; Hou, T.; Chen, H.; Yeh, L.; Chiu, F.-C.; Muller, A. J.; Hadjichristidis, N. Lower Critical Ordering Transition of Poly-(Ethylene Oxide)-Block-Poly(2-Vinylpyridine). *Macromolecules* **2011**, 44, 440–443.
- (64) Watanabe, M.; Hirakimoto, T.; Mutoh, S.; Nishimoto, A. Polymer Electrolytes Derived from Dendritic Polyether Macromonomers. *Solid State Ionics* **2002**, *148* (3–4), 399–404.
- (65) Sun, B.; Mindemark, J.; Edström, K.; Brandell, D. Polycarbonate-Based Solid Polymer Electrolytes for Li-Ion Batteries. *Solid State Ionics* **2014**, 262, 738–742.
- (66) Zhang, J.; Yang, J.; Dong, T.; Zhang, M.; Chai, J.; Dong, S.; Wu, T.; Zhou, X.; Cui, G. Aliphatic Polycarbonate-Based Solid-State Polymer Electrolytes for Advanced Lithium Batteries: Advances and Perspective. *Small* **2018**, *14* (36), 1–16.
- (67) Pesko, D. M.; Webb, M. A.; Jung, Y.; Zheng, Q.; Miller, T. F.; Coates, W.; Balsara, N. P. Universal Relationship between Conductivity and Solvation-Site Connectivity in Ether-Based Polymer Electrolytes. *Macromolecules* **2016**, *49*, 5244–5255.